Effective Hamiltonian for protected edge states in graphene

R. Winkler and H. Deshpande

Effective Hamiltonian for protected edge states in graphene

R. Winkler[1, 2] and H. Deshpande[1]

[1]*Department of Physics, Northern Illinois University, DeKalb, Illinois 60115, USA*
[2]*Materials Science Division, Argonne National Laboratory, Argonne, Illinois 60439, USA*
(Dated: June 2, 2017)

Edge states in topological insulators (TIs) disperse symmetrically about one of the time-reversal invariant momenta Λ in the Brillouin zone (BZ) with protected degeneracies at Λ. Commonly TIs are distinguished from trivial insulators by the values of one or multiple topological invariants that require an analysis of the bulk band structure across the BZ. We propose an effective two-band Hamiltonian for the electronic states in graphene based on a Taylor expansion of the tight-binding Hamiltonian about the time-reversal invariant M point at the edge of the BZ. This Hamiltonian provides a faithful description of the protected edge states for both zigzag and armchair ribbons though the concept of a BZ is not part of such an effective model. We show that the edge states are determined by a band inversion in both reciprocal and real space, which allows one to select Λ for the edge states without affecting the bulk spectrum.

A topological insulator (TI) is an insulator in the bulk with topologically protected edge states that cross the gap so that the edges are conducting. This concept was first introduced by Kane and Mele using a simple tight-binding (TB) model for the band structure of graphene.[1,2] Since then a wide range of materials with these properties have been identified in two and three dimensions (2D and 3D).[3,4] TIs can be distinguished from trivial insulators without topological edge states by the values of one or multiple topological invariants that require an analysis of the bulk band structure across the Brillouin zone (BZ). In that sense TIs are considered conceptually different from other problems in solid state physics that permit a description local in $\mathbf{k}$ space.

The first experimental verification of topologically protected edge states was achieved for HgTe/CdTe quantum wells (QWs)[5] following a theoretical proposal by Bernevig, Hughes and Zhang[6] based on a simple effective Hamiltonian, today known as BHZ model. Since then the BHZ model has been used in a wide range of studies. Liu et al. showed[7] that it also describes the edge states in InAs/GaSb QWs. Zhou et al. demonstrated[8] that the BHZ model can be solved exactly, yielding analytical expressions for the edge states in HgTe/CdTe QWs, see also Ref. 9. We do not question the deep insights that have emerged from the classification of solids based on topological invariants. But Zhou's work[8] raises the question to what extent TIs permit a description local in $\mathbf{k}$ space.[10] Is the concept of a BZ a necessary prerequisite for protected edge states in a TI? Graphene with its simple TB description[11] has served as an archetype for TIs,[1,2,12] despite the fact that its intrinsic SOC has been found to be small.[13] We show here that a Taylor expansion of the graphene TB model about the time-reversal invariant $\mathbf{M}$ point of the BZ (with $\mathbf{M} \equiv -\mathbf{M}$) yields an effective Hamiltonian that provides a faithful description local in $\mathbf{k}$ space of the protected edge states in both zigzag and armchair graphene ribbons. While the proposed model is quite different from the more familiar BHZ Hamiltonian, these models share a range of conceptual features, some of which previously unrecognized,
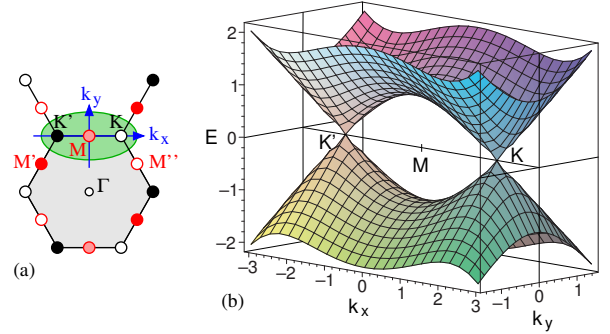

FIG. 1. (Color online) (a) Bulk BZ of graphene. The region captured by the effective Hamiltonian (1) is marked in green. (b) Bulk band structure $E(\mathbf{k})$ of the Hamiltonian (1) in the limit $\lambda_v = \lambda_i = \lambda_r = 0$.

which suggests that these features are common among TIs. Quite generally[1] the edge states in TIs disperse symmetrically about one of the time-reversal invariant momenta (TRIM) Λ with protected degeneracies at Λ. We show that this Λ is determined by a band inversion in both reciprocal and real space, which allows one to select Λ without affecting the bulk spectrum.

In the following our conventions for the TB Hamiltonian follow Refs. 1 and 2, see also Ref. 14. While the graphene BZ has two inequivalent points $\mathbf{K}$ and $\mathbf{K}'$ (with $\mathbf{K} \not\equiv -\mathbf{K}$), we have three inequivalent points $\mathbf{M}$, $\mathbf{M}'$ and $\mathbf{M}''$, see Fig. 1(a). Expanding the TB Hamiltonian for the graphene π bonds about $\mathbf{M} = (0, 2\pi/\sqrt{3})$, the effective Hamiltonian up to second order in $\mathbf{k} = (k_x, k_y)$ becomes

$$
\begin{aligned}
H_M(\mathbf{k}) = & \left[\left(1 - \tfrac{1}{4}k_x^2 + \tfrac{1}{12}k_y^2 \right) \sigma_z + \tfrac{2}{\sqrt{3}}k_y \sigma_y \right] t - \sigma_x \lambda_v \\
& - 4k_x s_z \sigma_x \lambda_i + \left[-\tfrac{2}{\sqrt{3}}s_x \sigma_y - \left(\tfrac{1}{2\sqrt{3}}k_y s_x + \tfrac{\sqrt{3}}{2}k_x s_y \right) \sigma_z \right. \\
& \left. + \left(\tfrac{1}{8}k_x^2 s_x - \tfrac{1}{4}k_x k_y s_y + \tfrac{5}{24}k_y^2 s_x \right) \sigma_y \right] \lambda_r,
\end{aligned}
\tag{1}
$$

where s_i denotes spin operators and σ_i are Pauli matrices. The first term describes the orbital motion characterized by the nearest-neighbor hopping parameter t (in
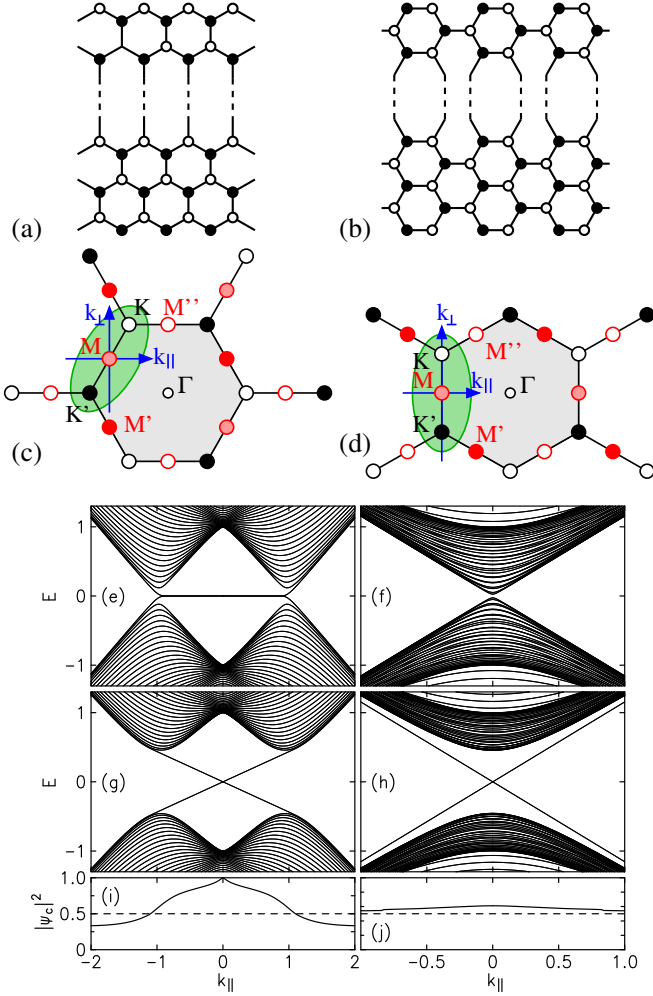
FIG. 2. (Color online) Crystal structure of a graphene ribbon with (a) zigzag and (b) armchair edges. Bulk BZ of graphene corresponding to (c) zigzag and (d) armchair ribbons. The region of the BZ captured by the Hamiltonian (1) is marked in green. Band structure $E(k_\parallel)$ of (e) zigzag and (f) armchair ribbons in the absence of SOC and (g), (h) for $\lambda_i = 0.2$. (i), (j) Squared magnitude of the up component of pseudospin σ_z of the lowest $E > 0$ bulk eigenstates. The width of the ribbons is $w = 40$ and we used $b_e = -10$.

the dispersion becomes [Fig. 1(b)]

$$E_\pm(\mathbf{k}) = \pm\sqrt{(1 - \tfrac{1}{4}k_x^2)^2 + k_y^2(\tfrac{3}{2} - \tfrac{1}{24}k_x^2) + \tfrac{1}{144}k_y^4}, \quad (2)$$

where the upper (lower) sign corresponds to the conduction (valence) band. For these bands the M point is a saddle point. For $k_y = 0$, the dispersion becomes $E_\pm(k_x, 0) = \pm(1 - \tfrac{1}{4}k_x^2)$ so that the bands touch at the points $(\pm 2, 0)$, which mimics the dispersion near the points K and K' of the BZ, the precise coordinates of which are $(\pm 2\pi/3, 0)$. Indeed, if we substitute $k_x \to k_x \pm 2$, the Hamiltonian (1) is unitarily equivalent to (ignoring Rashba SOC for simplicity)

$$H_K(\mathbf{k}) = \pm k_x \sigma_x - \tfrac{2}{\sqrt{3}}k_y \sigma_y + (\tfrac{1}{4}k_x^2 - \tfrac{1}{12}k_y^2)\sigma_x$$
$$+ \lambda_v \sigma_z \pm 4(2 \pm k_x)s_z\lambda_i\sigma_z. \quad (3)$$

For small $\mathbf{k}$, Eq. (3) is close to the Dirac Hamiltonian $H_D = \tfrac{\sqrt{3}}{2}(\pm k_x\sigma_x - k_y\sigma_y)$ obtained via a Taylor expansion of the TB Hamiltonian about K.[13] The Hamiltonian (1) thus captures the essential features of the graphene multivalley band structure for both the conduction and valence band near the entire line $K - M - K'$, so that it provides an alternative approach to *valleytronics*.[17] Unlike H_D, the Hamiltonian (1) accounts for time reversal symmetry in a natural way.

To discuss edge states we consider graphene ribbons with zigzag [Fig. 2(a)] and armchair edges [Fig. 2(b)]. The electronic states in these ribbons near energy $E = 0$ emerge from the states in 2D graphene which are highlighted in green in Fig. 2(c) and (d).

First we focus on zigzag edges [Fig. 2(a)]. We denote the wave vector for the motion along (perpendicular to) the direction of the ribbon as $k_\parallel$ ($k_\perp$). Ignoring SOC, zigzag edges give rise to a gapped spectrum around $k_\parallel = 0$ with edge states appearing in the center of the gap.[18] These results are readily rederived by means of Hamiltonian (1), where a suitable coordinate transformation gives the Hamiltonian

$$H_z(\mathbf{k}) = (1 - \tfrac{1}{6}k_\perp^2 + \tfrac{1}{2\sqrt{3}}k_\perp k_\parallel)\sigma_z - (\tfrac{1}{\sqrt{3}}k_\perp + k_\parallel)\sigma_y. \quad (4)$$

We model the edges as potential steps $b\sigma_z$ with $b \equiv b_g = 0$ inside the ribbon and $b \equiv b_e \neq 0$ outside. In the end we may consider the limit $|b_e| \to \infty$ so that the wave functions vanish at the edges.[8,9]

The edge states resulting from Eq. (4) are shown in Fig. 2(e). In these calculations, we used the barrier parameter $b_e = -10$. Having $b_e < 0$ implies a band inversion at the graphene edge.[19] A simple confinement $b_e > 0$ results in the spectrum shown in Fig. 3(b), where we have the same bulk spectrum as in Fig. 2(e), but the edge states appear for $|k_\parallel| \gtrsim 1$. The latter type of spectrum is obtained in TB calculations for ribbons with bearded edges,[20–22] see Fig. 3(a).

We can understand the results in Figs. 2(e,g) and 3 by looking at the *bulk* eigenstates of the ribbon. Figures 2(i) and (j) show the squared magnitude of the up
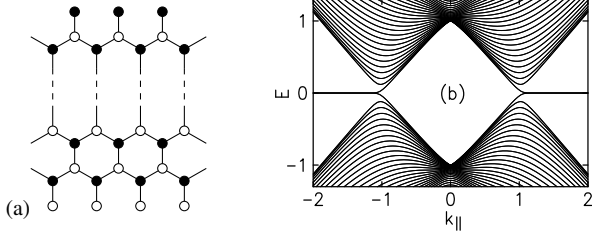
the following $t \equiv 1$). The second term describes a staggered sublattice potential weighted by λ_v.[1,2] The third term gives the intrinsic spin-orbit coupling (SOC) proportional to λ_i. The fourth term describes the Rashba SOC weighted by λ_r. In the following, $\mathbf{q}$ refers to wave vectors in the BZ whereas $\mathbf{k}$ denotes wave vectors relative to the expansion point $\mathbf{q}_0$ of the effective Hamiltonian, i.e., $\mathbf{q} = \mathbf{q}_0 + \mathbf{k}$.

First we discuss the properties of H_M in the absence of SOC. Unlike the Bloch states at the K point,[16] the Bloch states at the M point are nonzero on both sublattices of the graphene structure so that here σ_z does not permit an interpretation as sublattice pseudospin. For $\lambda_v = 0$,

FIG. 3. (a) Crystal structure of a graphene ribbon with bearded edges. (b) Band structure $E(k_\parallel)$ of the ribbon in the absence of SOC. The width of the ribbon is $w = 40$ and we used $b_e = +10$.

FIG. 4. Band structure $E(q_\parallel)$ of a BHZ ribbon with $a = 1$ and $b = 0.5$. (a) $m = -0.5$ yields a gapped spectrum without edge states. (b) For $m = +0.5$, the usual boundary conditions at the edges of the ribbon[23] yield edge states near $q_\parallel = 0$. (c) Dropping one of the basis states $s \pm p$ in the outermost layers of the ribbon yields edge states near the boundary $q_\parallel = \pi$ of the BZ. Projection of the lowest bulk conduction band states and uppermost bulk valence band states on the subspace of positive energies at (d), (e) $q_\parallel = 0$ and (f) $q_\parallel = \pi$.

component of the pseudospin σ_z [in the basis of Eq. (4)] of the lowest $E > 0$ bulk eigenstates as a function of $k_\parallel$ (with very similar results also for $b_e > 0$). Figure 2(i) indicates that for small $|k_\parallel|$ these states are predominantly pseudospin-up. Yet around $|k_\parallel| \simeq 1$ (reflecting the K point of bulk graphene) the character of these states changes from dominantly spin-up to spin-down. The electronic states thus see effective band edges as a function of $k_\parallel$ that show a band inversion in reciprocal space around $|k_\parallel| \simeq 1$. This inversion results in robust edge states for either $|k_\parallel| \lesssim 1$ [Fig. 2(e)] or $|k_\parallel| \gtrsim 1$ [Figs. 3(b)], depending on the sign of b_e. For graphene zigzag ribbons it is, of course, well-known that different boundary conditions at the edges as in Figs. 2(a) and Figs. 3(a) yield these different edge states.[18,20,22] Yet it is, indeed, a *common* feature of TIs that they show a band inversion in reciprocal space between the TRIM $\Lambda = 0$ and $\Lambda = \pi$ of the 1D BZ, so that we have edge states around either $\Lambda = 0$ or $\Lambda = \pi$. Choosing appropriate boundary conditions at the edges of the ribbon thus allows one to select the location of edge states in the 1D BZ while keeping the bulk spectrum unaffected.

To illustrate this point, Fig. 4 shows the band structure of a ribbon using the TB regularization of the BHZ model based on a square lattice with one s and p orbital per unit cell.[6,23] The Hamiltonian is $H = \begin{pmatrix} h(\mathbf{q}) & 0 \\ 0 & h^*(-\mathbf{q}) \end{pmatrix}$ with $h(\mathbf{q}) = \mathbf{d} \cdot \boldsymbol{\sigma}$, $d_x = a \sin q_x$, $d_y = a \sin q_y$, and $d_z = m - 2b(2 - \cos q_x - \cos q_y)$. In Fig. 4(a) the mass parameter m is negative, yielding a trivial regime without edge states. For $m > 0$ and using the usual boundary conditions,[23] we get conducting edge states near the center $q_\parallel = 0$ of the 1D BZ [Fig. 4(b)]. Alternatively, we may consider the unitarily equivalent problem with hybridized basis orbitals $s + p$ and $s - p$. Dropping one of these orbitals in the outermost layers of the ribbon yields edge states near the boundary $q_\parallel = \pi$ of the 1D BZ, while the bulk spectrum remains unchanged [Fig. 4(c)]. For the trivial case in Fig. 4(a) the bulk eigenstates do not show band inversion as a function of $q_\parallel$ [Fig. 4(d)], whereas the nontrivial cases in Figs. 4(b) and (c) show band inversion [Figs. 4(e) and (f)]. Similar results also hold for graphene ribbons with armchair edges, see the Appendix.

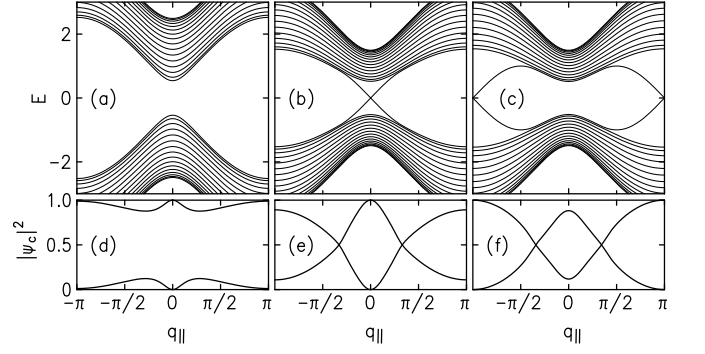We return to the effective Hamiltonian (1). The numerical calculations presented in this work use a quadra-

ture method as described in Refs. 24 and 25, which automatically ensures the proper matching conditions for the multi-spinor wave function at the edges of the ribbon. The numerical results can be confirmed by analytical calculations similar to those in Refs. 8 and 9. In particular, the limit of hard walls $b_e \to -\infty$ yields for the edge state at $k_\parallel = 0$ of a semi-infinite graphene sheet at $r_\perp \geq 0$

$$\psi_z(r_\perp) = \begin{pmatrix} 1 \\ 1 \end{pmatrix} (e^{-\kappa_+ r_\perp} - e^{-\kappa_- r_\perp}), \quad \kappa_\pm \equiv \sqrt{3}(1 \pm i), \ (5)$$

and $\psi_z(r_\perp < 0) = 0$. The corresponding eigenenergy is $E = 0$. The full expressions for finite b_e, finite thickness of the ribbon and finite $k_\parallel$ are more complicated so that they are not reproduced here. Yet such calculations confirm that no edge states exist around $k_\parallel = 0$ for $b_e > 0$.

For a ribbon with armchair edges [Fig. 2(b)] and neglecting SOC, the effective Hamiltonian becomes

$$H_a(\mathbf{k}) = \left(1 - \tfrac{1}{4}k_\perp^2 + \tfrac{1}{12}k_\parallel^2\right)\sigma_z - \tfrac{2}{\sqrt{3}}k_\parallel \sigma_y, \qquad (6)$$

see Fig. 2(d). The 1D spectrum resulting from $H_a(\mathbf{k})$ is shown in Fig. 2(f). Here we have no edge states and in the limit of wide ribbons the spectrum becomes gapless. These results are in line with the findings in Ref. 18, keeping in mind that the bulk K and K' points are folded to the point $q_\parallel = 0$ of the 1D BZ for armchair ribbons.

Previously Brey and Fertig[26] used the graphene Dirac Hamiltonian H_D to obtain the edge states of 1D ribbons emerging from the states near the K point of 2D graphene,[27] i.e., their model gives the edge states for wave vectors close to the valence band maximum and conduction band minimum in Figs. 2(e) and (f). The present approach is different from this earlier work as it yields the edge states in the entire region in between the points K and K' of the bulk band structure including the robust crossing at $k_\parallel = 0$, consistent with
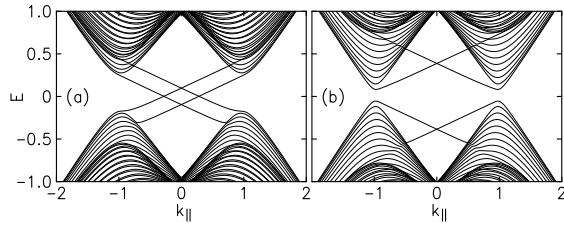
FIG. 5. Band structure $E(k_\parallel)$ of zizag ribbons for $\lambda_i = 0.09$ and $\lambda_r = 0.05$. The sublattice staggering is (a) $\lambda_v = 0.1$ and (b) $\lambda_v = 0.4$. The width of the ribbon is $w = 40$ and we used $b_e = -10$. Compare Fig. 1 of Ref. 1.

the TB description.[18] Effective Hamiltonians based on a Taylor expansion of the band structure are often low-energy Hamiltonians that are valid only in the vicinity of the expansion point.[24,28] Yet this is not an inherent constraint.[29]

Next we discuss the effect of SOC. First we consider $\lambda_r = 0$. The intrinsic SOC $\propto \lambda_i$ opens a gap $16\lambda_i\sqrt{1 - 16\lambda_i^2} \approx 16\lambda_i$ in the bulk spectrum of the Hamiltonian (1). In the TB model this gap becomes $6\sqrt{3}\lambda_i$.[2] For $\lambda_i \neq 0$ the edge states in a zigzag or armchair ribbon remain two-fold degenerate at $k_\parallel = 0$ which reflects the fact that these states originate from the time-reversal invariant M point of the graphene BZ. This aspect is thus readily captured by the Hamiltonian (1), as demonstrated in Figs. 2(g) and (h).

Both the intrinsic SOC $\propto \lambda_i$ and the staggering $\propto \lambda_v$ open a gap in the bulk spectrum of the Hamiltonian (1). Yet it follows immediately from Eq. (3) that the gap closes for $\lambda_v = \pm 8\lambda_i$. Consistent with the TB results in Ref. 1 this set of parameters describes the phase boundary between the topologically trivial regime with an even number of edge states and the nontrivial regime with an odd number of edge states crossing the bulk gap. Similarly, Rashba SOC $\propto \lambda_r$ induces such a phase transition when it competes with the intrinsic SOC. Figure 5 illustrates this point for zigzag ribbons. Here the staggering $\lambda_v = 0.1$ [Fig. 5(a)] gives rise to edge states crossing the gap, whereas $\lambda_v = 0.4$ [Fig. 5(b)] results in an ordinary insulator. These calculations are in very good agreement with the TB results in Fig. 1 of Ref. 1.

Finally we comment on the general robustness of the edge states, which is a major aspect motivating the interest in topological insulators.[3,4] It was pointed out in Ref. 2 that the edge states at $\Lambda \pm k_\parallel$ form Kramers doublets so that elastic backscattering from a weak random potential preserving time reversal symmetry is forbidden. This argument applies also to the effective Hamiltonian (1). Yet if the electron states are modeled by means of the low-energy Dirac Hamiltonian H_D, the two time-reversed valleys at K and K' are described via a discrete valley pseudospin degree of freedom, that makes it difficult to incorporate intervalley scattering in a general way. For the Hamiltonian (1) pairs of time-reversed states are connected by continuous paths in the Hilbert space of this

Hamiltonian so that it is well-suited to incorporate intervalley scattering, though a detailed study of this point is beyond the scope of the present work.

In conclusion, the effective Hamiltonian (1) based on an expansion of the graphene TB Hamiltonian about the time-reversal invariant M point provides an accurate description of the topologically protected edge states in graphene, although the concept of a BZ is not part of such an effective model. Similar effective Hamiltonians can be derived via a Taylor expansion of, e.g., the graphene TB Hamiltonian about the BZ center $q = 0$ or the TB-regularized BHZ Hamiltonian about the TRIM $\mathbf{q} = (\pi, 0)$ [suitable for a description of the "inverted" protected edge states in Fig. 4(c)]. We may expect that similar Hamiltonians exist also for other topologically protected systems in both 2D and 3D. Our work may inspire further research on necessary conditions for the formation of protected edge states and robust level degeneracies. For example, numerical studies based on the effective 8×8 Kane Hamiltonian have shown that a 2D Dirac semimetal with robust level crossings can be realized in HgTe-CdTe quantum wells when the well thickness is varied.[30] Also, the effective models proposed here open an avenue for studying these systems under perturbations such as homogeneous or inhomogeneous[12] magnetic and electric fields or strain which may break the periodicity of the ideal crystal structure[31] so that it is more difficult to incorporate such effects in atomistic calculations.

Appendix: Ribbons with Bearded Edges

We show here that the protected edge states in graphene ribbons with bearded zigzag [Fig. 6(a)] and bearded amrchair edges [Fig. 6(b)] can be analyzed in complete analogy with Fig. 2. The electronic states in these ribbons near energy $E = 0$ emerge from the states in the 2D BZ of graphene which are highlighted in green in Fig. 6(c) and (d). First we discuss these ribbons in the absence of SOC. For bearded zigzag edges, the effective Hamiltonian becomes

$$H_{bz}(\mathbf{k}) = \left(1 - \tfrac{1}{4}k_\parallel^2 + \tfrac{1}{12}k_\perp^2\right)\sigma_z + \tfrac{2}{\sqrt{3}}k_\perp\sigma_y. \quad \text{(A.1)}$$

The resulting dispersion is shown in Fig. 6(e). For bearded armchair edges, the effective Hamiltonian becomes

$$H_{ba}(\mathbf{k}) = (1 - \tfrac{1}{6}k_\parallel^2 + \tfrac{1}{2\sqrt{3}}k_\parallel k_\perp)\sigma_z - (\tfrac{1}{\sqrt{3}}k_\parallel + k_\perp)\sigma_y. \quad \text{(A.2)}$$
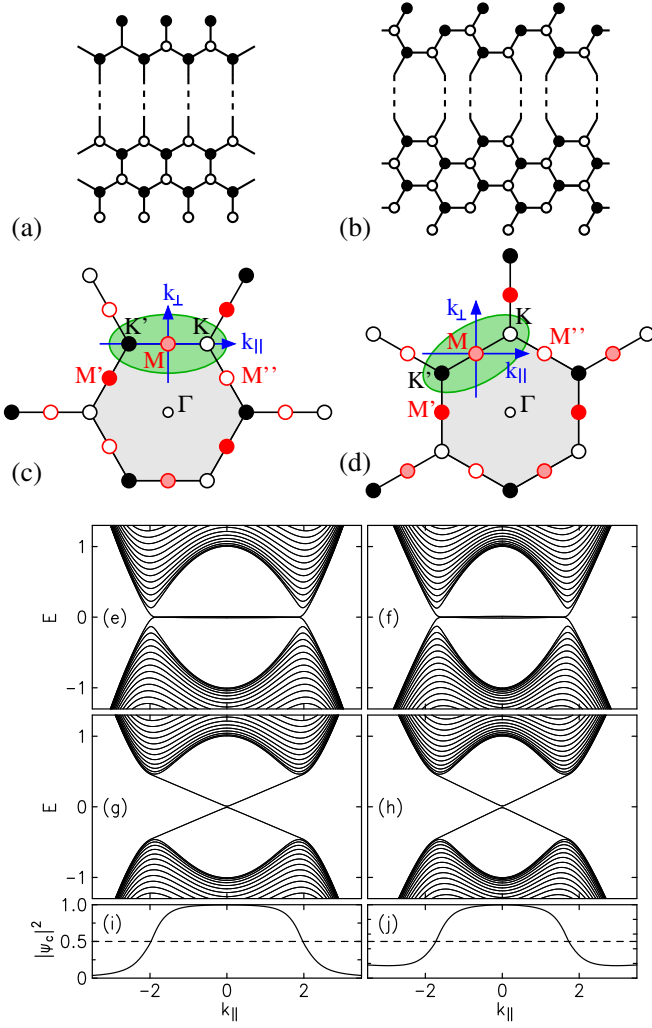
FIG. 6. (Color online) Crystal structure of a graphene ribbon with (a) bearded zigzag and (b) bearded armchair edges. Bulk BZ of graphene corresponding to (c) bearded zigzag and (d) bearded armchair ribbons. The region of the BZ captured by the Hamiltonian (1) is marked in green. Band structure $E(k_\parallel)$ of (e) bearded zigzag and (f) bearded armchair ribbons in the absence of SOC and (g), (h) for $\lambda_i = 0.2$. (i), (j) Squared magnitude of the up component of pseudospin σ_z of the lowest $E > 0$ bulk eigenstates. The width of the ribbons is $w = 40$ and we used $b_e = -10$.

The resulting dispersion is shown in Fig. 6(f). Similiar to Figs. 2(g) and (h), intrinsic SOC opens a gap in the bulk band structure of bearded ribbons. Using $b_e < 0$ we get the protected edge states shown in Figs. 6(g) and (h). Similar to Figs. 2(e)-(h), the results in Figs. 6(e)-(h) are in very good agreement with TB calculations for the ribbon geometries in Figs. 6(a) and (b). We note that similar to Figs. 4(b) and (c) the bulk spectra in Figs. 2(e), (g) and Figs. 6(e), (g) are the same, independent of the spectra of the edge states.

Figures 3(b) (obtained for $b_e > 0$) and 6(e) (obtained for $b_e < 0$) refer to the same bearded ribbon shown in Fig. 6(a). For this ribbon, the protected edge states disperse symmetrically about the TRIM $\Lambda = 0$ of the 1D BZ. An essential difference between the effective Hamiltonians underlying these figures thus lies in the fact that only the expansion point **M** in Fig. 6(c) is mapped onto $\Lambda = 0$ of the 1D BZ, thus yielding a robust model for the protected edge states of bearded zigzag ribbons, as demonstrated by Fig. 6(g).

More generally, a 2D TI has four TRIM Λ that are mapped pairwise on the two 1D-TRIM $\Lambda = 0$ and $\Lambda = \pi$ of the corresponding TI ribbon. The edge states may disperse about either $\Lambda = 0$ or $\Lambda = \pi$, and we need to choose the expansion point of the effective Hamiltonian accordingly for a robust description of the protected edge states.

[1] C. L. Kane and E. J. Mele, Phys. Rev. Lett. **95**, 146802 (2005).

[2] C. L. Kane and E. J. Mele, Phys. Rev. Lett. **95**, 226801 (2005).

[3] M. Z. Hasan and C. L. Kane, Rev. Mod. Phys. **82**, 3045 (2010).

[4] X.-L. Qi and S.-C. Zhang, Rev. Mod. Phys. **83**, 1057 (2011).

[5] M. König, S. Wiedmann, C. Brüne, A. Roth, H. Buhmann, L. W. Molenkamp, X.-L. Qi, and S.-C. Zhang, Science **318**, 766 (2007).

[6] B. A. Bernevig, T. L. Hughes, and S.-C. Zhang, Science **314**, 1757 (2006).

[7] C. Liu, T. L. Hughes, X.-L. Qi, K. Wang, and S.-C. Zhang, Phys. Rev. Lett. **100**, 236601 (2008).

[8] B. Zhou, H.-Z. Lu, R.-L. Chu, S.-Q. Shen, and Q. Niu, Phys. Rev. Lett. **101**, 246807 (2008).

[9] E. B. Sonin, Phys. Rev. B **82**, 113307 (2010).

[10] Effective models using a Taylor expansion of the band structure are based on the assumption that the resulting model can describe the states near the Fermi energy. They would generally fail to describe both "topological"

and "trivial" (nontopological) properties of a material if we have bands in other parts of the Brillouin zone near the Fermi energy.

[11] P. R. Wallace, Phys. Rev. **71**, 622 (1947).

[12] F. D. M. Haldane, Phys. Rev. Lett. **61**, 2015 (1988).

[13] A. H. Castro Neto, F. Guinea, N. M. R. Peres, K. S. Novoselov, and A. K. Geim, Rev. Mod. Phys. **81**, 109 (2009).

[14] To match the conventions in Ref. 15, the intrinsic SOC term in Eq. (1) must be multiplied by a factor $-1/2\sqrt{3}$ and the Rashba term by $-1/\sqrt{3}$.

[15] R. Winkler and U. Zülicke, Phys. Rev. B **82**, 245313 (2010).

[16] K. S. Novoselov, A. K. Geim, S. V. Morozov, D. Jiang, M. I. Katsnelson, I. V. Grigorieva, S. V. Dubonos, and A. A. Firsov, Nature **438**, 197 (2005).

[17] J. Tworzydło, I. Snyman, A. R. Akhmerov, and C. W. J. Beenakker, Phys. Rev. B **76**, 035411 (2007).

[18] M. Fujita, K. Wakabayashi, K. Nakada, and K. Kusakabe, J. Phys. Soc. Jpn. **65**, 1920 (1996).

[19] B. A. Volkov and O. A. Pankratov, JETP Lett. **42**, 178 (1985).

[20] D. J. Klein, Chem. Phys. Lett. **217**, 261 (1994).

[21] S. Ryu and Y. Hatsugai, Phys. Rev. Lett. **89**, 077002 (2002).

[22] B. A. Bernevig, *Topological Insulators and Topological Superconductors* (Princeton University Press, Princeton, NJ, 2013).

[23] J. K. Asbóth, L. Oroszlány, and A. Pályi, *A Short Course on Topological Insulators* (Springer, Cham, 2016).

[24] R. Winkler, *Spin-Orbit Coupling Effects in Two-Dimensional Electron and Hole Systems* (Springer, Berlin, 2003).

[25] R. Winkler and U. Rössler, Phys. Rev. B **48**, 8918 (1993).

[26] L. Brey and H. A. Fertig, Phys. Rev. B **73**, 235411 (2006).

[27] Similar to the present work, boundary conditions played also an important role in Ref. 26. Yet the nature of these boundary conditions was very different from the boundary conditions used here. Reference 26 treated the edges as hard walls. As H_D is linear in momentum we cannot require that both spinor components vanish simultaneously at the boundaries.

[28] G. Bastard, *Wave Mechanics Applied to Semiconductor Heterostructures* (Les Editions de Physique, Les Ulis, 1988).

[29] M. Cardona and F. H. Pollak, Phys. Rev. **142**, 530 (1966).

[30] R. Winkler, L. Y. Wang, Y. H. Lin, and C. S. Chu, Solid State Commun. **152**, 2096 (2012).

[31] G. L. Bir and G. E. Pikus, *Symmetry and Strain-Induced Effects in Semiconductors* (Wiley, New York, 1974).